Acta Crystallographica Section A
Foundations of Crystallography
ISSN 0108-7673

Received 10 January 2012
Accepted 11 April 2012

A practical study of the electron-density-map variance

Carmelo Giacovazzo* and Annamaria Mazzone

Institute of Crystallography – CNR, Via G. Amendola, 122/O 70126 Bari, Italy. Correspondence e-mail: carmelo.giacovazzo@ic.cnr.it

An algorithm is described for the calculation of the variance of the electron density *via* fast Fourier transform. The main features of the ratio *electron density/standard deviation* are described; it is shown that such a ratio may be considered a useful criterion for estimating, on an absolute scale, the quality of an electron-density map, no matter the quality of the model and the data resolution. In some way, it is a good estimate of the confidence one should have in the reliability of the proposed structure. The ratio was tested both for observed and for difference Fourier syntheses, in order to control the usefulness of the criterion for the most popular maps in crystallography.

1. Symbols and abbreviations

In the following, papers I and II refer, respectively, to Giacovazzo & Mazzone (2011) and Giacovazzo *et al.* (2011).
$F = \sum_{j=1}^{N} f_j \exp(2\pi i \mathbf{h}\mathbf{r}_j) = |F| \exp(i\varphi)$: structure factor of the target structure.
$F_p = \sum_{j=1}^{p} f_j \exp(2\pi i \mathbf{h}\mathbf{r}'_j) = |F_p| \exp(i\varphi_p)$, where $\mathbf{r}'_j = \mathbf{r}_j + \Delta\mathbf{r}_j$: structure factor of the model structure.
$\mathbf{C}_s \equiv (\mathbf{R}_s, \mathbf{T}_s)$ sth symmetry operator ($\mathbf{C}_s\mathbf{r} \equiv \mathbf{R}_s\mathbf{r} + \mathbf{T}_s$): $\mathbf{R}_s$ and $\mathbf{T}_s$ are the rotational and translational matrices, respectively.
n: number of the symmetry operators for the target and for the model structure.
$\sum_N = \sum_{j=1}^{N} f_j^2$, $\sum_p = \sum_{j=1}^{p} f_j^2$, where p is the number of atoms in the model structure.
$E = A + iB = R\exp(i\varphi)$, $E_p = A_p + iB_p = R_p \exp(i\varphi_p)$, $R = |F|/\sum_N^{1/2}$, $R_p = |F_p|/\sum_N^{1/2}$.
$\rho(\mathbf{r}) = (2/V)\sum_{\mathbf{h}>0} |F_\mathbf{h}| \cos(2\pi\mathbf{h}\cdot\mathbf{r} - \varphi_\mathbf{h})$: general expression for an electron-density map. The term of order zero is omitted. By $\mathbf{h} > 0$ it is meant that the summation is over one half of the reciprocal space (only one member of each Friedel pair is included in the summation).
$\mathrm{var}_\rho(\mathbf{r}) = \langle[\rho(\mathbf{r})]^2\rangle - [\langle\rho(\mathbf{r})\rangle^2]$: variance of the ρ map in a point $\mathbf{r}$.
$D_i(x) = I_i(x)/I_0(x)$, I_i is the modified Bessel function of order i.
$D = \langle\cos(2\pi\mathbf{h}\Delta\mathbf{r})\rangle$: the average is performed per resolution shell.
$\sigma_A = D(\Sigma_p/\Sigma_N)^{1/2}$.
$\sigma_R^2 = \langle|\mu|^2\rangle/\sum_N$, $\langle|\mu|^2\rangle$ is the measurement error and σ_R^2 is its normalized expression.
$e = 1 + \sigma_R^2$.
$m = \langle\cos(\varphi - \varphi_p)\rangle = I_1(X)/I_0(X)$, where $X = 2\sigma_A R R_p \times (e - \sigma_A^2)^{-1}$.
$s = \sin\theta/\lambda$.
$m_{\mathbf{ch}} = 0.5 + 0.5\tanh(X/2)$.
EDM: electron-density modification.
CORR: correlation between the model and the target electron-density maps.

2. Introduction

The mathematical expression of the variance of a Fourier synthesis at any point of the unit cell and for any space group has been recently established (see papers I and II). The basic hypotheses are very general:

(*a*) A model structure is available, no matter its correlation with the target structure.

(*b*) Each phase φ is distributed around φ_p according to the von Mises distribution

$$M(\varphi; X, \varphi_p) = [2\pi I_0(X)]^{-1} \exp[X\cos(\varphi - \varphi_p)]. \qquad (1)$$

(*c*) Standard deviations of the observed diffraction amplitudes [say $\sigma(|F_\mathbf{h}|)$] may be taken into account (see Coppens & Hamilton, 1968; Rees, 1976) and combined with the variance contribution arising from phase uncertainty.

The final expression for the variance is:

$$\mathrm{var}\rho(\mathbf{r}) = TH_1 + TH_2(\mathbf{r}) + TD(\mathbf{r}), \qquad (2)$$

where

$$TH_1 = \frac{2}{V^2}\sum_{\mathbf{h}>0}(1 - m_\mathbf{h}^2)[|F_\mathbf{h}|^2 + \sigma^2(|F_\mathbf{h}|)],$$

$$TH_2(\mathbf{r}) = \frac{2}{V^2}\sum_{\mathbf{h},\mathrm{ind}}[|F_\mathbf{h}|^2(1 - m_\mathbf{h}^2) + \sigma^2(|F_\mathbf{h}|)] \times \sum_{s\neq q=1}^{n}\cos\{2\pi\mathbf{h}[(\mathbf{C}_s - \mathbf{C}_q)\mathbf{r}]\},$$

$$TD(\mathbf{r}) = -\frac{2}{V^2}\sum_{\mathbf{h},\mathrm{ind}}\Big(\big\{|F_{\mathbf{h}}|^2[m_{\mathbf{h}}^2 - D_2(X_{\mathbf{h}})] - \sigma^2(|F_{\mathbf{h}}|)\big\} \times \sum_{s,q=1}^{n}\cos[2\varphi_p(\mathbf{h}) - 2\pi\mathbf{h}(\mathbf{C}_s + \mathbf{C}_q)\mathbf{r}]\Big).$$

For centric space groups the corresponding expression is

$$\mathrm{var}\rho(\mathbf{r}) = \frac{1}{V^2}\sum_{\mathbf{h},\mathrm{ind}}[|F_{\mathbf{h}}|^2(1 - m_{c\mathbf{h}}^2) + \sigma^2(|F_{\mathbf{h}}|)] \times \sum_{s,q=1}^{n}\cos[2\pi\mathbf{h}(\mathbf{C}_s - \mathbf{C}_q)\mathbf{r}]. \quad (3)$$

The subscript 'ind' in the symbol of summation indicates that **h** varies over the set of symmetry-independent reflections.

If CORR < 1, the contribution to the variance provided by measurement errors is negligible.

Equation (2) shows that the variance is the sum of three components: (i) The constant and positive term TH_1: it does not vary from point to point and depends on the correlation between the model and target structures. (ii) The term TH_2: it varies from point to point, does not depend on the model and is strictly connected with the *implication transformations method* (see Pavelčík, 1988; Pavelčík *et al.*, 1992 and literature quoted therein), a very important tool for Patterson deconvolution. (iii) The term TD: it varies from point to point, depends on the model phases and on the observed moduli.

This paper is of an applicative nature and has two main purposes: firstly, to describe an algorithm for the calculation of the variance *via* FFT (fast Fourier transform) techniques, an indispensable tool for protein crystallography, and, secondly, to study the features of the ratio

$$\rho(\mathbf{r})/\sigma_\rho(\mathbf{r}), \quad (4)$$

where $\sigma_\rho(\mathbf{r}) = [\mathrm{var}\rho(\mathbf{r})]^{1/2}$. The reason for this second application is the following.

In daily crystallographic work, particularly in protein crystallography, the standard deviation σ_d of the pixel intensity distribution of an electron-density map is calculated. It is tacitly assumed that pixels with $\rho(\mathbf{r}) > n\sigma_d$, and n sufficiently large, provide the most reliable information on the atomic positions in the unit cell. It is, however, impossible to state the absolute confidence one should have in the map reliability. Indeed σ_d^2 is not an estimate of the variance of the map because (*a*) it is a fixed parameter, which does not vary with the pixel position, while the variance varies from point to point, and (*b*) σ_d and σ_ρ are anticorrelated (the first diminishes and the second increases when CORR improves) when plotted against resolution (see Giacovazzo & Mazzone, 2011; Fig. 3). Such undesired features of σ_d do not allow one to assume $\rho(\mathbf{r})/\sigma_d$ as a 'signal-to-noise' ratio: we will show that this meaning may be associated with the ratio in equation (4).

3. About the main features of the ratio $\rho(\mathbf{r})/\sigma_\rho(\mathbf{r})$

A condition for the practical usefulness of the variance is its computability *via* FFT. The necessary algorithm is described in the Appendix.

The variance theory described in papers I and II suggests that, no matter the type of electron density (observed, difference, hybrid), the quality of the density (poor or accurate) in a given point of the map may be estimated *via* the ratio in equation (4). In this section we describe how equation (4) varies as a function of the structure under examination, the quality of the model and data resolution. We will also show that equation (4) is a good estimate of the confidence one should have in the reliability of the proposed structure.

Structures with heavy atoms (denoted below by HA) are expected to show distributions different from light-atom structures; equally, as an effect of the solvent, proteins may show different features with respect to small- or medium-size molecules. Accordingly, we used as experimental tests four crystal structures (three with data at atomic or quasi-atomic resolution) which are considered good representatives of the different categories:

(i) BCDIMP, a medium-size organic molecule [$C_{55}H_{76}N_4O_{37}$, space group $P2_1$, 0.82 Å data resolution; Impellizzeri *et al.* (2000)].

(ii) PHERO (PDB code 2erl, 40 residues, space group $C2$, HA = 7 S in the asymmetric unit, 1.0 Å data resolution).

(iii) ASPAR (PDB code 1fy2, 220 residues, space group $C2$, HA = 4 S, Cd, data resolution 1.2 Å).

(iv) CALMOPB (PDB code 1n0y, 166 residues, space group $C2$, HA = 14 Pb, As, 1.75 Å data resolution).

For each test structure we calculated the value of equation (4) in each pixel of the map at different steps of the phasing process, each step corresponding to a different average phase error $\langle|\Delta\varphi|\rangle$ (calculated with respect to the published structure). The ρ/σ_ρ axis has been subdivided in bins, and for each bin the pixel percentage (say PERC) with the given value of ρ/σ_ρ has been calculated. The corresponding histograms are shown in Figs. 1–4; since ρ/σ_ρ may be considered as an estimate of the 'signal-to-noise' ratio (S/N), in the figures we will report PERC *versus* S/N for different $\langle|\Delta\varphi|\rangle$ values (for clarity, the PERC axis is on a log scale).

The main features may be summarized as follows:

(*a*) All the curves show their maximum at S/N $\sim$ 0, independently of the quality of the model. The corresponding pixels lie far away from the current peaks in the map, mostly inside the solvent region when the model is sufficiently good.

(*b*) The distributions [equation (4)] are strongly asymmetrical with respect to the S/N axis: the asymmetry increases with the quality of the model. This feature is quite reasonable: when the model improves, the intensities of the positive peaks (on average) increase while the (average) variance decreases, so allowing curves in Figs. 1–4 to gradually reach higher and higher values of S/N. In these conditions the electron-density map provides an accurate description of the atomic positions and of the electron distribution.

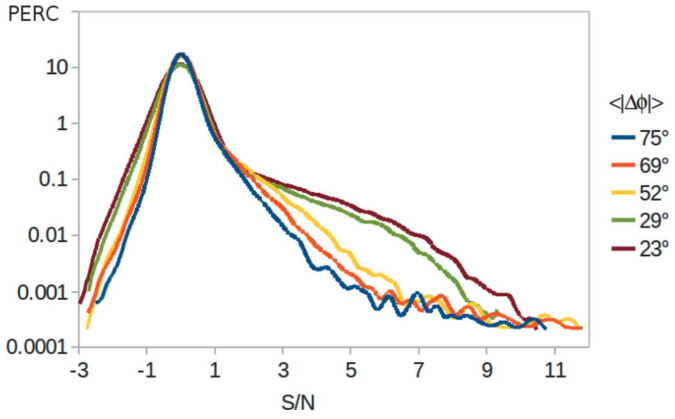

Figure 1
BCDIMP: pixel percentage (PERC) with a given S/N value, for different values of the average phase error $\langle|\Delta\varphi|\rangle$.

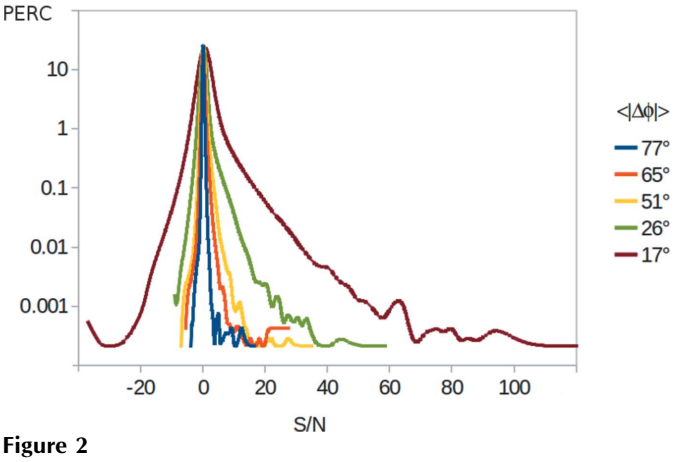

Figure 2
PHERO: pixel percentage (PERC) with a given S/N value, for different values of the average phase error $\langle|\Delta\varphi|\rangle$.

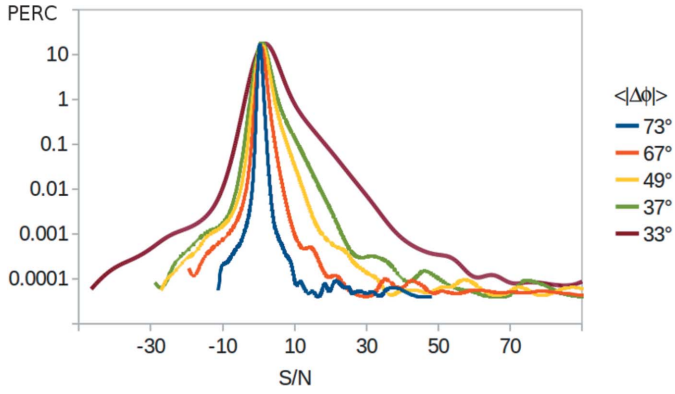

Figure 3
ASPAR: pixel percentage (PERC) with a given S/N value, for different values of the average phase error $\langle|\Delta\varphi|\rangle$.

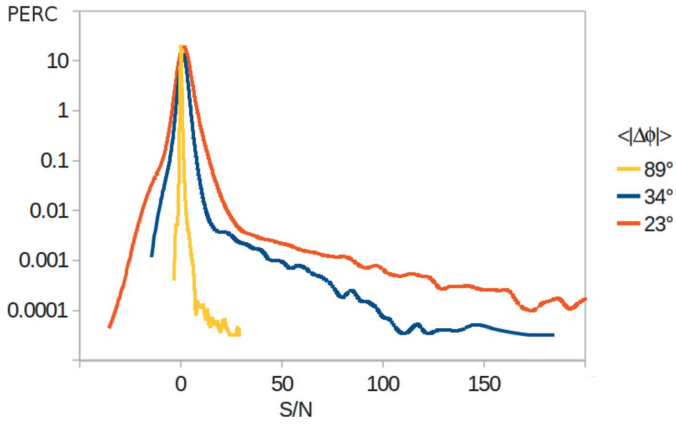

Figure 4
CALMOPB: pixel percentage (PERC) with a given S/N value, for different values of the average phase error $\langle|\Delta\varphi|\rangle$.

Since F_{000} has not been included in the set of Fourier coefficients, each electron-density map shows regions with negative values of ρ, and therefore of S/N. If CORR increases, the main peaks in the maps become more intense, the corresponding ripples become deeper (the deepness of a ripple depends on the intensity of the related peak, while ripple periodicity depends on data resolution), and the value of |S/N| in correspondence with the ripples may increase. This result suggests that high-quality maps characterize well the ripples closest to the main peaks: high values of |S/N| are associated with them. That should not be a surprise: indeed, if a positive peak is characterized well by a high-quality electron density, the negative ripples must also be characterized well, because there is a physical relation between them; it is not by chance that a strong covariance between a positive peak and its ripples has been found by Altomare *et al.* (2012).

(*c*) The S/N ratio rarely reaches values larger than 5 when the structure model is bad. Values that exceed this correspond to heavy-atom positions, which are located well *via* Patterson techniques (the phasing techniques we used to start the phasing process; Burla *et al.*, 2006; Caliandro *et al.*, 2008).

(*d*) When heavy atoms are present and the model is sufficiently good, the S/N ratio may reach values larger than 100 at the pixels coincident with or very close to the heavy-atom positions (indeed, heavy-atom peaks, very likely, are more correctly positioned than light-atom peaks). Let us consider the curves in Figs. 1–4 corresponding to the best models. The reader will notice that the maximum value of S/N for BCDIMP, a light-atom structure, is 11.8; it is 133 for PHERO, occurring in correspondence with the 7 sulfur positions; 287 for ASPAR, attained at Cd positions; 249 for CALMOPB, in correspondence with the Pb positions.

(*e*) The results in point (*d*) introduce resolution effects on the S/N ratio. Its average value is expected to decrease when the resolution becomes worse. Accordingly, the maximum value of S/N for CALMOPB is smaller than that obtained for ASPAR, in spite of the larger (with respect to Cd) atomic number of Pb.

(*f*) To provide the reader with an overall view of the pixel distribution as a function of the model quality, we show in Fig. 5 the cumulative distribution for ASPAR: C_P is the percentage of the pixels with $\rho(\mathbf{r})/\sigma_\rho(\mathbf{r})$ smaller than a given S/N value. We see that about 70% of the pixels have an S/N smaller than 2 for

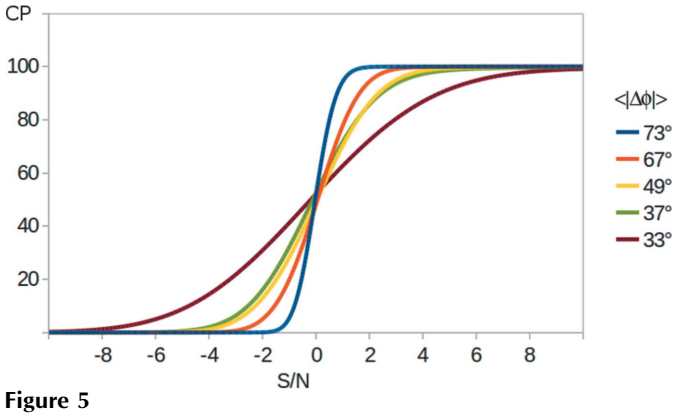

Figure 5
ASPAR: C_P is the percentage of pixels with $\rho(\mathbf{r})/\sigma_\rho(\mathbf{r})$ smaller than a given S/N value.

the best structural model; the percentage progressively increases when the model becomes poorer.

The above tests define well the good features of the ratio $\rho(\mathbf{r})/\sigma_\rho(\mathbf{r})$ when $\rho(\mathbf{r})$ is an observed electron density (*i.e.* calculated by using observed moduli and model phases). To extend our investigation to difference or hybrid electron-density maps we consider for BCDIMP three difference maps (say $\Delta\rho$) calculated by using Read (1986) coefficients $mR - \sigma_A R_p$. Even though new difference syntheses have very recently been proposed (Burla *et al.*, 2010), Read coefficients are better documented and are far superior to unweighted difference Fourier maps (the coefficients m and σ_A are today statistically calculated *via* standard programs). We used:

(i) Two model structures, with $\langle|\Delta\varphi|\rangle$ = 55 and 65°, respectively; the first difference map is shown in Fig. 6 and the second in Fig. 7. The two models are obtained by eliminating suitable groups of atoms from the published structure. Only pixels with an intensity larger than $3\sigma_d$ are shown in the figures. It is easily seen that the two maps are not of high quality, the first being slightly better than the second. Indeed, for both the maps, there are positive densities both on the model atoms and in wrong positions: only a fraction of the difference electron-density peaks lies on the atoms belonging to the difference structure. In this situation we should expect a distribution of $\Delta\rho(\mathbf{r})/\sigma_\rho(\mathbf{r})$ not exceeding some modest threshold value. This is really what we obtain. In Fig. 8 we show the distribution of $\Delta\rho(\mathbf{r})/\sigma_\rho(\mathbf{r})$ for both the models: for them S/N is always smaller than 2.6, thus suggesting the modest confidence we should have in the proposed difference structure.

(ii) A model structure with $\langle|\Delta\varphi|\rangle$ = 22°, obtained by eliminating from the published structure eight atoms (3 O and 5 C) and by introducing four false atomic positions (3 C and 1 O). The difference Fourier map clearly identifies both the missed and the false additional positions (see Fig. 9). The first eight positive maxima of $\Delta\rho(\mathbf{r})/\sigma_\rho(\mathbf{r})$ lie in correspondence with the eight missed atoms: S/N varies from 9.12 in correspondence with an O, down to 6.2 in correspondence with a C. For the next positive maximum S/N = 1.34, well separated from the preceding eight values. The first four negative minima correspond to the four false atomic positions: S/N varies from 13.3 in correspondence with O, down to 9.12 for a C atom. The next negative minimum has S/N = 3.47.

It may be interesting to compare the values of S/N obtained above for the difference Fourier map with those obtained for an observed Fourier synthesis (by using the same model structure). In accordance with the theoretical predictions, the maximum value of S/N in the observed Fourier map is 24.0, much larger than 9.12, the maximum of the difference map. The first maxima in the observed map lie in correspondence with the well positioned atoms: S/N goes from 9.6 to 6.4 for the missed atoms, and from 9.2 to 5.8 for the false ones.

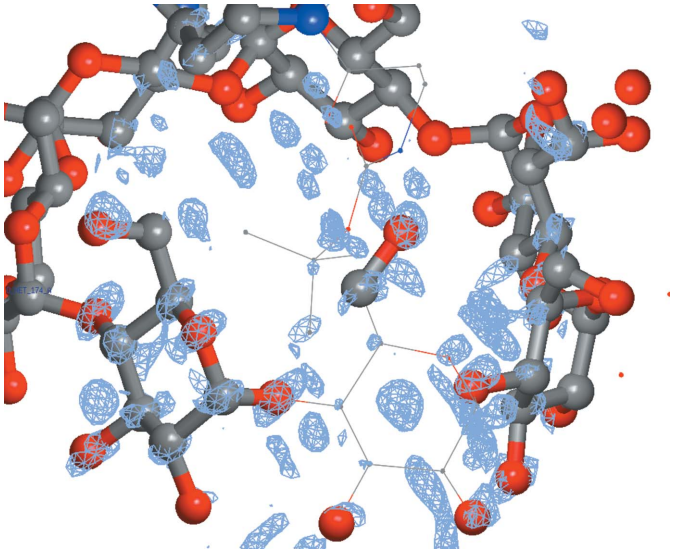

Figure 6
BCDIMP: model structure ($\langle|\Delta\varphi|\rangle$ = 55°; represented by sticks and balls) superimposed with the main peaks of the difference electron density; only map pixels with an intensity larger than $3\sigma_d$ are taken into account. The atoms of the difference structure are represented in simple plotting style.

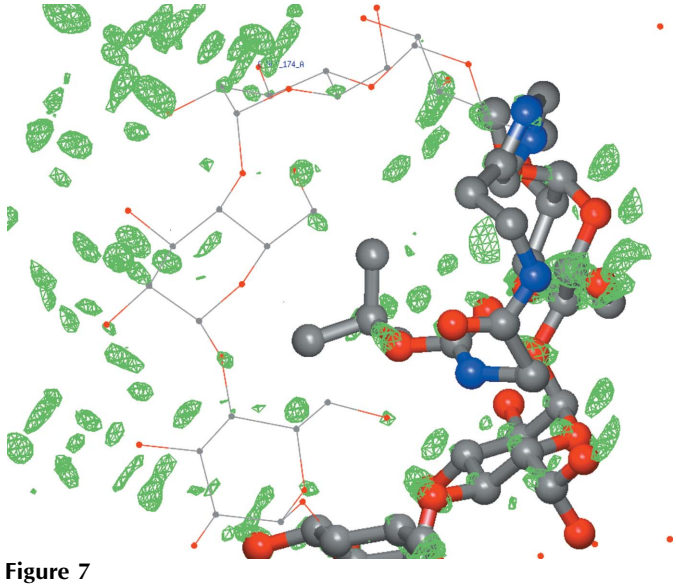

Figure 7
BCDIMP: model structure ($\langle|\Delta\varphi|\rangle$ = 65°; represented by sticks and balls) superimposed with the main peaks of the difference electron density; only map pixels with an intensity larger than $3\sigma_d$ are taken into account. The atoms of the difference structure are represented in simple plotting style.

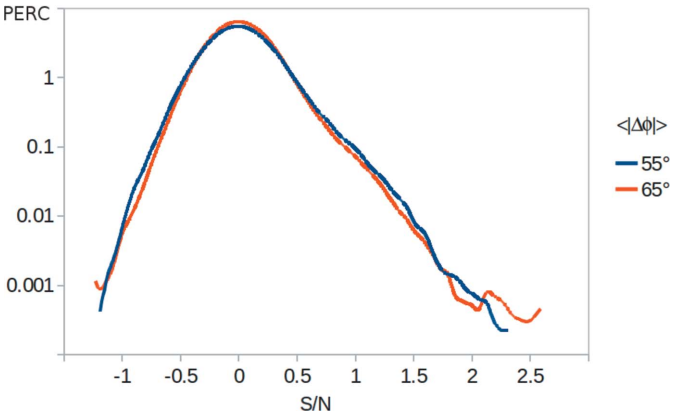

Figure 8
BCDIMP: difference electron-density map. Pixel percentage (PERC) with a given S/N value, for different values of the average phase error $\langle|\Delta\varphi|\rangle$.

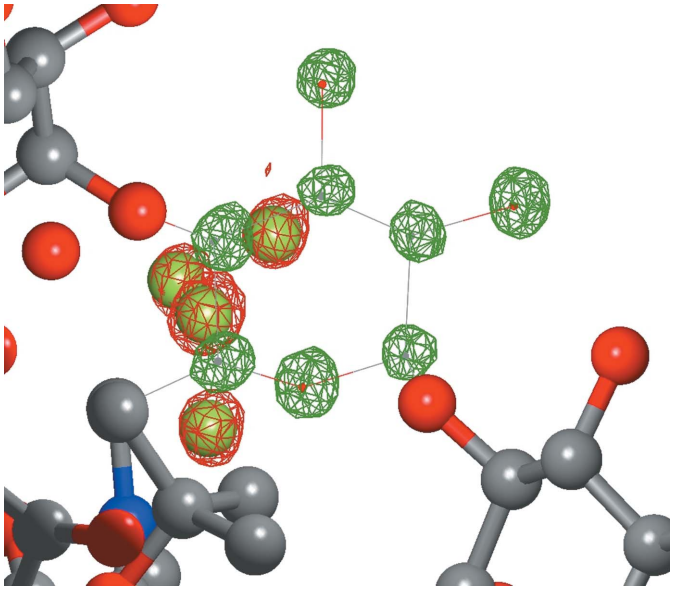

Figure 9
BCDIMP: $\Delta\rho(\mathbf{r})/\sigma_\rho(\mathbf{r})$ map calculated for a model for which $\langle|\Delta\varphi|\rangle = 22^\circ$; only map pixels with an intensity larger than $5\sigma_d$ are taken into account. Green wire frames correspond to positive S/N values, red frames to negative S/N values.

In conclusion, missed and false atoms may be recognized, *via* difference Fourier synthesis, with about the same S/N values obtained by using an observed Fourier synthesis (both the maps use the same amount of information).

4. Conclusions

An algorithm has been described which enables, for an electron-density map, the calculation of the corresponding variance *via* fast Fourier transform techniques. This result allows one to rapidly compute the ratio *electron density/standard deviation* at each point of the electron-density map; the ratio may be considered a good estimate of the confidence one should have in the reliability of the map at that point. Our applications to four test structures show the good features of the criterion, valid for different qualities of the model structure. It seems able to set on an absolute reliability scale the density at each pixel of the electron-density map by taking into full account model quality, chemical composition and data resolution.

APPENDIX *A*
Variance calculation *via* FFT

A condition for the practical usefulness of the variance is its computability *via* FFT. As shown in paper II, equation (2) may be transformed into

$$\begin{aligned}\mathrm{var}\,\rho(\mathbf{r}) = {} & \frac{4}{V^2}\sum_{\mathbf{h},\mathrm{ind}}[(1-m_{\mathbf{h}}^2)+\sigma^2(|F_{\mathbf{h}}|)] \\ & \times \sum_{s,q=1}^{n} F_{\mathbf{hR}s}\exp(-2\pi i\mathbf{hR}_s\mathbf{r})F_{-\mathbf{hR}q}\exp(2\pi i\mathbf{hR}_q\mathbf{r}) \\ & - \frac{4}{V^2}\sum_{\mathbf{h},\mathrm{ind}}[m_{\mathbf{h}}^2 - D_2(X_{\mathbf{h}}) - \sigma^2(|F_{\mathbf{h}}|)] \\ & \times \sum_{s,q=1}^{n} F_{\mathbf{hR}s}\exp(-2\pi i\mathbf{hR}_s\mathbf{r})F_{\mathbf{hR}q}\exp(-2\pi i\mathbf{hR}_q\mathbf{r}). \quad (5)\end{aligned}$$

If we rewrite the first term on the right-hand side of equation (5) [say $TH_1 + TH_2(\mathbf{r})$] in the form

$$\begin{aligned}\frac{4}{V^2}\sum_{\mathbf{h},\mathrm{ind}}[1-m_{\mathbf{h}}^2+\sigma^2(|F_{\mathbf{h}}|)]\sum_{s,q=1}^{n}|F_{\mathbf{hR}s}F_{-\mathbf{hR}q}| \\ \times\exp[-2\pi i\mathbf{h}(\mathbf{T}_s-\mathbf{T}_q)]\exp[-2\pi i\mathbf{h}(\mathbf{R}_s-\mathbf{R}_q)\mathbf{r}]\end{aligned}$$

and we define

$$\mathbf{h}(\mathbf{R}_s-\mathbf{R}_q) = \mathbf{H}_{s,q}, \quad (6)$$

then we can rewrite $TH_1 + TH_2(\mathbf{r})$ as

$$\frac{4}{V^2}\sum_{\mathbf{H}s,q} A_{\mathbf{H}s,q}\exp(-2\pi i\mathbf{H}_{s,q}\mathbf{r}),$$

where

$$\begin{aligned}A_{\mathbf{H}s,q} = {} & \sum_{\mathbf{h},\mathrm{ind}}[1-m_{\mathbf{h}}^2+\sigma^2(|F_{\mathbf{h}}|)]\sum_{s,q=1}^{n}|F_{\mathbf{hR}s}F_{-\mathbf{hR}q}| \\ & \times\exp[-2\pi i\mathbf{h}(\mathbf{T}_s-\mathbf{T}_q)] \\ = {} & n_{\mathbf{h}}\sum_{\mathbf{h},\mathrm{ind}}[1-m_{\mathbf{h}}^2+\sigma^2(|F_{\mathbf{h}}|)]|F_{\mathbf{h}}|^2 \\ & + 2\sum_{s<q=1}^{n}|F_{\mathbf{h}}|^2\cos 2\pi\mathbf{h}(\mathbf{T}_s-\mathbf{T}_q)] \quad (7)\end{aligned}$$

and $n_{\mathbf{h}}$ is the multiplicity of the reflection $\mathbf{h}$. The sum over the $\mathbf{h}$ reflections is extended to all the unique $\mathbf{h}$ which satisfy equation (6).

Let us now rearrange the *TD* expression in equation (3) as

$$TD(\mathbf{r}) = -\frac{4}{V^2}\sum_{\mathbf{h},\mathrm{ind}}[m_{\mathbf{h}}^2 - D_2(X_{\mathbf{h}}) - \sigma^2(|F_{\mathbf{h}}|)] \times \sum_{s,q=1}^{n} F_{\mathbf{hR}s}\exp(-2\pi i\mathbf{hR}_s\mathbf{r})F_{\mathbf{hR}q}\exp(-2\pi i\mathbf{hR}_q\mathbf{r}). \quad (8)$$

If we define

$$\mathbf{h}(\mathbf{R}_s + \mathbf{R}_q) = \mathbf{K}_{s,q}, \quad (9)$$

we can rewrite equation (8) as

$$TD(\mathbf{r}) = \frac{4}{V^2}\sum_{\mathbf{K}s,q} B_{\mathbf{K}s,q}\exp(-2\pi i\mathbf{K}_{s,q}\mathbf{r}), \quad (10)$$

where

$$B_{\mathbf{K}s,q} = \sum_{\mathbf{h},\mathrm{ind}}[m_{\mathbf{h}}^2 - D_2(X_{\mathbf{h}}) - \sigma^2(|F_{\mathbf{h}}|)] \times \sum_{s,q=1}^{n} |F_{\mathbf{hR}s}F_{\mathbf{hR}q}|\exp[2i\varphi_{\mathbf{h}} - 2\pi i\mathbf{h}(\mathbf{T}_s + \mathbf{T}_q)]. \quad (11)$$

The sum over the reflections in equation (11) is extended to all the unique **h** which satisfy equation (9). Finally

$$\mathrm{var}\rho(\mathbf{r}) = \frac{4}{V^2}\left[\sum_{\mathbf{H}s,q} A_{\mathbf{H}s,q}\exp(-2\pi i\mathbf{H}_{s,q}\mathbf{r}) + \sum_{\mathbf{K}s,q} B_{\mathbf{K}s,q}\exp(-2\pi i\mathbf{K}_{s,q}\mathbf{r})\right]. \quad (12)$$

In accordance with the above results, computing the variance map *via* an FFT series implies the previous calculation of the terms $A_{\mathbf{H}sq}$ and $B_{\mathbf{H}sq}$, and their subsequent use as coefficients of the series [equation (12)]. In general, owing to equations (6) and (9), the number of **H** and **K** indices is smaller than the number of measured reflections (indeed, for most symmetry operators several **h** may correspond to the same **H** or to the same **K**), but **H** and **K** indices span a reciprocal-space volume much larger than the reflections **h**. This property obliges the user to allocate supplementary memory for the calculation of the variance, an action particularly undesired when large proteins are treated. Alternatively, one could decide not to involve in equation (12) **H** and **K** reflections with a resolution larger than the experimental one: but in this case the quality of the variance map becomes lower. In our calculations we extended the reciprocal-space volume to include all **H** and **K** vectors of interest.

References

Altomare, A., Cuocci, C., Giacovazzo, C., Moliterni, A. & Rizzi, R. (2012). *Acta Cryst.* A**68**, 244–255.

Burla, M. C., Caliandro, R., Carrozzini, B., Cascarano, G. L., De Caro, L., Giacovazzo, C., Polidori, G. & Siliqi, D. (2006). *J. Appl. Cryst.* **39**, 728–734.

Burla, M. C., Caliandro, R., Giacovazzo, C. & Polidori, G. (2010). *Acta Cryst.* A**66**, 347–361.

Caliandro, R., Carrozzini, B., Cascarano, G. L., De Caro, L., Giacovazzo, C., Mazzone, A. & Siliqi, D. (2008). *J. Appl. Cryst.* **41**, 548–553.

Coppens, P. & Hamilton, W. C. (1968). *Acta Cryst.* B**24**, 925–929.

Giacovazzo, C. & Mazzone, A. (2011). *Acta Cryst.* A**67**, 210–218.

Giacovazzo, C., Mazzone, A. & Comunale, G. (2011). *Acta Cryst.* A**67**, 368–382.

Impellizzeri, G., Pappalardo, G., D'Alessandro, F., Rizzarelli, E., Saviano, M., Iacovino, R., Benedetti, E. & Pedone, C. (2000). *Eur. J. Org. Chem.* **6**, 1065–1076.

Pavelčík, F. (1988). *Acta Cryst.* A**44**, 724–729.

Pavelčík, F., Kuchta, L. & Sivý, J. (1992). *Acta Cryst.* A**48**, 791–796.

Read, R. J. (1986). *Acta Cryst.* A**42**, 140–149.

Rees, B. (1976). *Acta Cryst.* A**32**, 483–488.